

1958APJ...128...465D

PHOTOELECTRIC PHOTOMETRY OF THE ANDROMEDA NEBULA IN THE U, B, V SYSTEM

GERARD DE VAUCOULEURS*

Lowell Observatory, Flagstaff, Arizona

Received May 28, 1958; revised July 10, 1958

ABSTRACT

An isophotic map of M31 in blue light was established by means of direct photoelectric scans spaced at $10'$ intervals in declination from $+39^{\circ}30'$ to $42^{\circ}30'$. The color distribution at selected declinations and the mean color indices in the U, B, V system were determined. The luminosity distribution in the central region was derived from earlier data reduced to the same system. The integrated magnitude and colors of M31 (exclusive of companions) within an area of 4.0 square degrees limited by the isophote $B_0 = 26.8$ mag/sec² are $m_0(B) = 4.39$, $B - V = +0.91$, $U - B = +0.50$; the probable errors are ± 0.02 mag. The position angle of the major axis is $37^{\circ}7' \pm 0^{\circ}2'$ (p.e.). The axial ratio reaches a minimum $(b/a)_m \approx 0.25$ near $2a = 100'$, where $B \approx 22.5$ mag/sec², corresponding to the outline of the main spiral arms. Allowing for the tilt of the equatorial plane on the line of sight, the true axial ratio of the flat component of M31 is $q = 0.042$, and the corresponding "thickness" of the spiral structure is about 0.8 kpc.

The luminosity profile along the major axis can be analyzed, after removal of the flat component ($B - V = +0.85$, $U - B = +0.4$) in terms of a spheroidal component ($B - V = +1.0$, $U - B = +0.6$) closely obeying the luminosity law typical of elliptical galaxies (de Vaucouleurs 1953); this spheroidal component contributes 24 per cent of the total luminosity in blue light; it dominates the luminosity distribution in the central regions up to $a \approx 30'$ and may become important again beyond $a \approx 3''$. The effective dimensions of the isophote within which is emitted half the total luminosity are $2a_e = 71'$, $b_e/a_e = 0.30$ with $B_e = 22.62$ mag/sec²; corresponding figures for the spheroidal component alone are $2a'_e = 35'$, $b'_e/a'_e = 0.6$, $B'_e = 22.86$ mag/sec². Comparison with the mass derived by M. Schmidt (1957*b*) leads to a mean apparent mass/luminosity ratio $j(B) = \mathfrak{M}/\mathfrak{L}_B = 24$. The mass of the spheroidal component derived from Minkowski's estimate of the velocity dispersion leads to an apparent mass/luminosity ratio $j'(B) = 70$. The mass of the flat component obtained by difference leads to an apparent mass/luminosity ratio $j''(B) = 6$.

I. INTRODUCTION

The Andromeda Nebula has previously been the subject of a number of fragmentary photometric studies (Stebbins and Whitford 1934; Redman and Shirley 1937; Holmberg 1950; Stebbins 1950; Hoag 1952; Fricke 1954; Baum and Schwarzschild 1955; Lindblad 1956). The recent Dutch work on the 21-cm H I line emission (van de Hulst, Raimond, and van Woerden 1957) has, however, emphasized the urgent need for new optical observations of the luminosity and color distribution over the entire area of the nebula in a well-defined photometric system (M. Schmidt 1957*b*). The present paper reports on the results of such observations which were undertaken at the suggestion of Dr. M. Schmidt and carried out in October and November, 1957, by means of the Lowell Observatory 21-inch reflector equipped with a photoelectric photometer kindly made available by Dr. H. L. Johnson.

II. INSTRUMENTAL AND OBSERVATIONAL DATA

The program included the determination of (a) a complete set of isophotes in blue light (B), from direct photoelectric scans at constant declinations regularly spaced at $10'$ intervals from $\delta = +39^{\circ}30'$ to $\delta = +42^{\circ}30'$; (b) the color distribution ($U - B$, $B - V$) at the declination δ_N of the nucleus and at declinations $\delta_N \pm 30'$ and $\delta_N \pm 60'$. From a and b the luminosity profiles along the main axes and the integrated magnitudes and colors can be derived.

The photometer was similar to the instrument used in the establishment of the

* Now at Harvard College Observatory, Cambridge, Massachusetts

standard U , B , V system (Johnson and Morgan 1953; Johnson 1955). The calibration of the amplifier steps is estimated to be good to ± 0.003 mag. (p.e.).

Preliminary trials were made in October with a 10-mm hole used for spot readings but this procedure was found too slow and unsatisfactory. In November a circular diaphragm of 5.5 mm placed in the focal plane at the Cassegrain focus (scale 1 mm = 25") was used for scanning. The effective diameters of the holes were carefully determined by recording and timing star transits at various declinations. The constants of the field diaphragms are listed in Table 1. The last column gives the conversion constant from the apparent magnitude measured through the hole to the corresponding surface brightness in magnitudes per square second of arc.

Two of Johnson's standard stars α Ari and ν And were used, the properties of which are given in Table 2. The p.e.'s of the magnitudes and colors are about ± 0.005 and ± 0.003 mag., respectively. The star ν And, being in the field of M31, was observed each

TABLE 1
INSTRUMENTAL CONSTANTS

Hole (mm)	Diameter	$2.5 \log A$ (mag)
5.5	$138^{\circ}0 \pm 0^{\circ}.5$	10.438 ± 0.005
10. . . .	$249^{\circ}.5 \pm 0^{\circ}.5$	11.722 ± 0.005

TABLE 2
STANDARD STARS

Star	Spectrum	V	$B - V$	$U - B$
α Ari.	K2 III	2.00	+1.15	+1.12
ν And . .	B2 V	4.53	-0.15	-0.58

night, usually both at the beginning and at the end of the run; α Ari was observed only on 2 nights each month to establish the color system. Only first-class nights were used, and observations were restricted to hour angles less than ± 4 hours, i.e., $\sec z < 1.45$, so that mean absorption coefficients could be used, viz.,

$$Q_y = 0.15 \text{ mag.}, \quad Q_b = 0.23 - 0.030 C_y, \quad Q_u = Q_b + 0.26.$$

The very small fluctuations in the mean absorption coefficient from night to night were taken care of by comparing the standard magnitudes of ν And with the observed values; nightly zero-point corrections averaging ± 0.01 mag. were applied accordingly. The mean B magnitude (outside the atmosphere) corresponding to 1 unit of deflection (hole 5.5) at $\sec z = 1$ for the mean color of M31 (Sec. VIII) was $B_1 = 15.346 \pm 0.004$ (p.e.). The main series of observations was secured in 6 nights (November 19-27, 1957). The image of the sky was allowed to drift in front of the field aperture at the diurnal rate; the Brown recorder was driven at the rate of 1 inch per 2 minutes of time, which gave a convenient scale of about 68 mm per degree on which the diameter of the scanning hole was represented by about 0.1 inch. A sample scan in blue light through the nucleus is shown in Figure 1; the maximum detectable extent of the nebula on the central scan was about 93'.

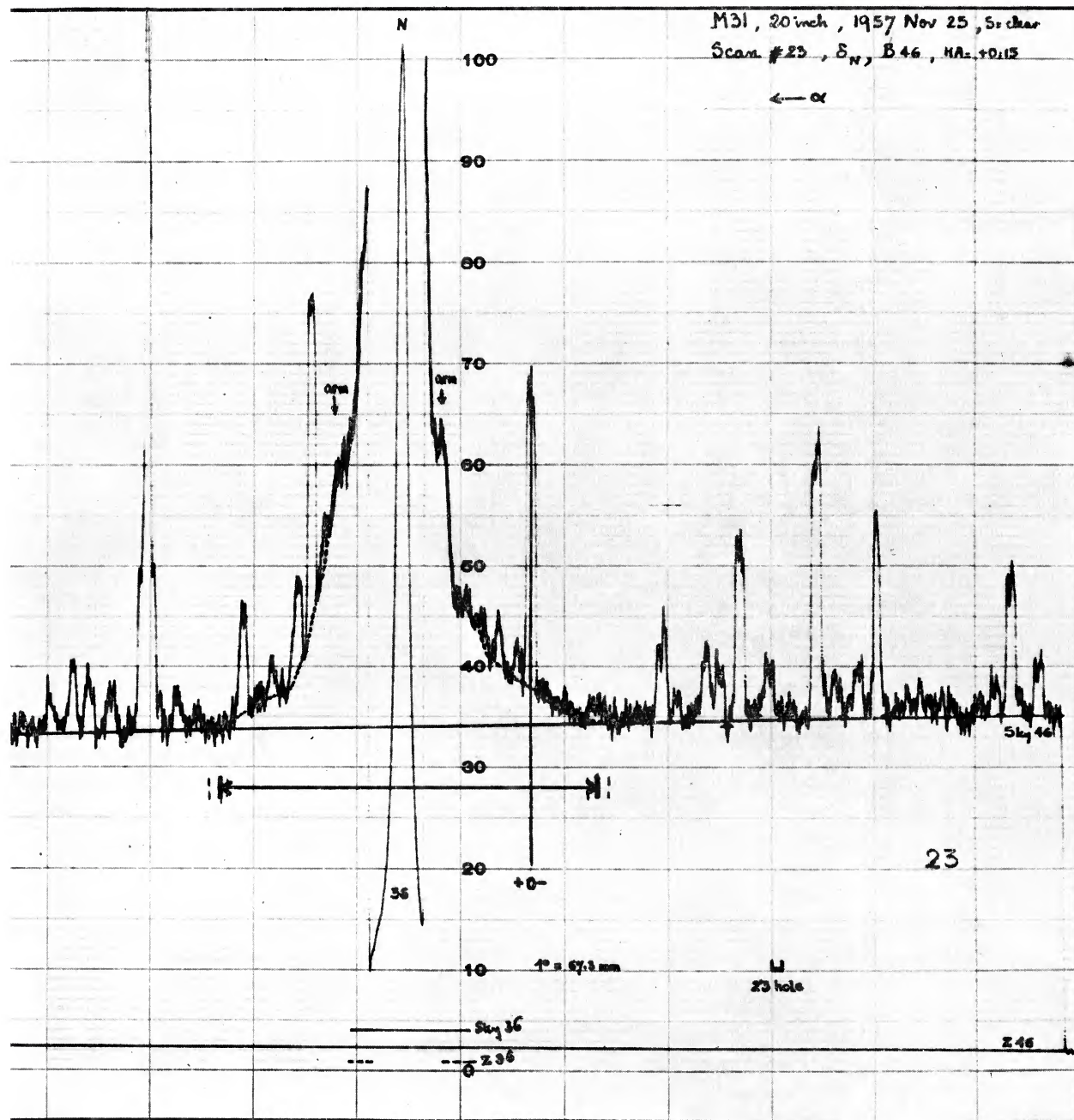


FIG. 1.—Sample east-west scan through the nucleus

III. MEASUREMENTS AND REDUCTION

As a matter of convenience, all scans were reduced to the zenith, which involved only small differential corrections, and the conversion to magnitudes was achieved by computing the surface brightness B_1 (in mag/sec² outside the atmosphere), corresponding to one unit of deflection at sec $z = 1.000$. Allowing for the aperture constant in Table 1, this brightness corresponds to

$$B_1 = 15.346 + 10.438 = 25.784 \pm 0.009 \text{ (p.e.) mag/sec}^2.$$

The p.e. includes those of (1) the aperture constant, (2) the standard magnitudes (± 0.005), (3) the standardization (± 0.004), and (4) the amplifier steps (± 0.003). An independent check on the calibration (Sec. V) leads to $B_1' = 25.80 \pm 0.05$ or 25.90 ± 0.04 , so that the value finally adopted for the zero point of the B magnitudes is

$$B_1 = 25.80 \pm 0.01 \text{ (p.e.)}.$$

The paths of the continuous scans at constant declination were accurately located on an enlargement from a Palomar 48-inch Schmidt plate by means of the field stars recorded on each tracing. In general, only one scan was obtained at each declination, except at $\delta = +61'0$ (2 scans) and at the declination of the nucleus (8 scans), which was usually recorded as a check at both the beginning and the end of each run.

The precise scale ratio between photograph and tracing was also determined at each declination from the star deflections, and a prominent star conveniently located was selected on each trace as a provisional origin for the scale of abscissae. All stars brighter than $m \approx 15$ and likely to contribute appreciably to the observed deflections were then identified through a detailed comparison of tracings and photographs. A continuous trace, defined mainly by the apparently undisturbed sections, was then drawn and completed by interpolation where necessary (Fig. 1); this curve was taken to represent the true luminosity profile of the nebula. A mean "blank"-sky level was defined by linear interpolation between similarly undisturbed regions well outside the nebula, and deflections above this reference level were read, in general, at 0.1-inch intervals (corresponding to the diameter of the scanning hole) or at 0.05-inch intervals where necessary to cover adequately such significant details as spiral arms or dark lanes.

The accuracy of the corrected deflections b can be judged from a comparison of the eight independent scans at the declination of the nucleus; the mean values B and average deviation $\epsilon(b)$ from the means are plotted in Figure 2. The average deviation is well represented by

$$\epsilon(b) = 0.40 + 0.030b,$$

so that the p.e. of the sky level is $(\text{p.e.})_0 = \pm 0.35$ or 1.3 per cent of the mean "blank"-sky deflection of 27 units. Since the sky level was determined independently on each tracing, and a total of about 20 scans was used to plot the isophotes, the p.e. of the mean sky level is of the order of ± 0.08 unit, equivalent to $B = 28.5$ mag/sec². The p.e. of the B surface brightness measured at any point of one tracing varies as shown in Figure 2 (*inset*).

IV. THE BLUE LIGHT-ISOPHOTES AND LUMINOSITY PROFILES

a) *Isophotes*

In the bright inner regions ($b \geq 4$ units, $B \leq 24.3$ mag/sec²), the isophotes were drawn at 0.25-mag. intervals through the individual observed points accurately located at each declination with respect to the reference star; photographs were used as a guide for the interpolation between adjacent scans. In the faint outer regions ($b < 4$), mean points from adjacent scans were used, and the isophotes were drawn at half-magnitude intervals by freehand interpolation between the observed points. The resulting isophotic

map is shown in Figure 3. The last "measured" isophote is No. 1, for which $b = 1.0$, $B_1 = 25.80 \text{ mag/sec}^2$; the outermost contour No. 0 outlines the region inside which a perceptible deflection could be associated with the nebula; a posteriori this was found to correspond roughly to $b \approx 0.4$, $B_0 \approx 26.8 \text{ mag/sec}^2$. Since the brighter part of M32 was not crossed by a scan, no isophotes are shown for it; the isophotes of NGC 205 are roughly indicated but are only approximate because of the large spacing of the scans and the low resolution. The estimated courses of the isophotes of M31 after removal of the disturbances due to the companions are shown by the thin dashed lines in Figure 3.

b) Main Axes

The location of the major axis of M31 was defined by the nucleus and by twenty equally spaced points, ten on each side of the nucleus (Fig. 3). Each of these points was determined as the mean center of the segments defined by the intersection with the

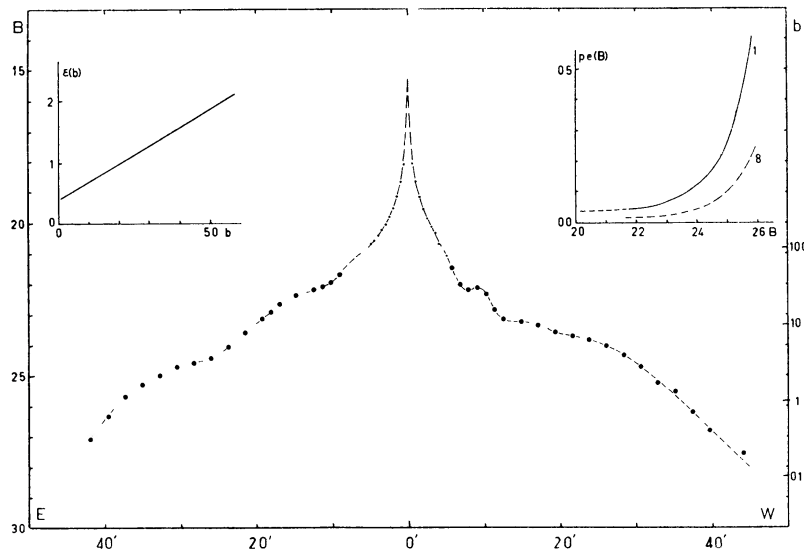


FIG 2—Luminosity distribution along the east-west central section from 8 scans in blue light. The inner region (*small dots*) is from unpublished observations by A. Hoag (1952). The scale is in mag/sec^2 (B , scale at left) and units of deflection (b , scale at right). *Left inset*: average deviation $\epsilon(b)$ of the 8 scans from their mean as a function of b . *Right inset*: probable error of B in magnitudes for 1 scan and for the mean of 8 scans as a function of B .

more regular isophotes of a parallel to a provisional minor axis. Each point is the average of from two to eight such centers, usually grouped within $1'-2'$ from their mean. The points lie very close to the straight line chosen as the most probable location of the major axis of M31; the only noticeable departures occur in the outermost regions, where the isophotes are poorly determined, and at about $30'$ south-preceding the nucleus, where a well-known local dissymmetry occurs in the spiral pattern, possibly caused by interaction with M32 (Schwarzschild 1954). The adopted major axis is in position angle

$$\text{p.a. (major axis)} = 37^{\circ}.7 \pm 0^{\circ}.2 \text{ (p.e.)}.$$

A previous determination by Hubble (1929) is $36^{\circ}.7$, by visual inspection of direct photographs. The description of the major axis given by Lindblad (1956) implies $39^{\circ}.0$.

c) Luminosity Profiles

The luminosity distributions along the major and minor axes, as derived from the intersections of the isophotes with the two main axes, are shown in Figure 4 and summarized in Table 3.

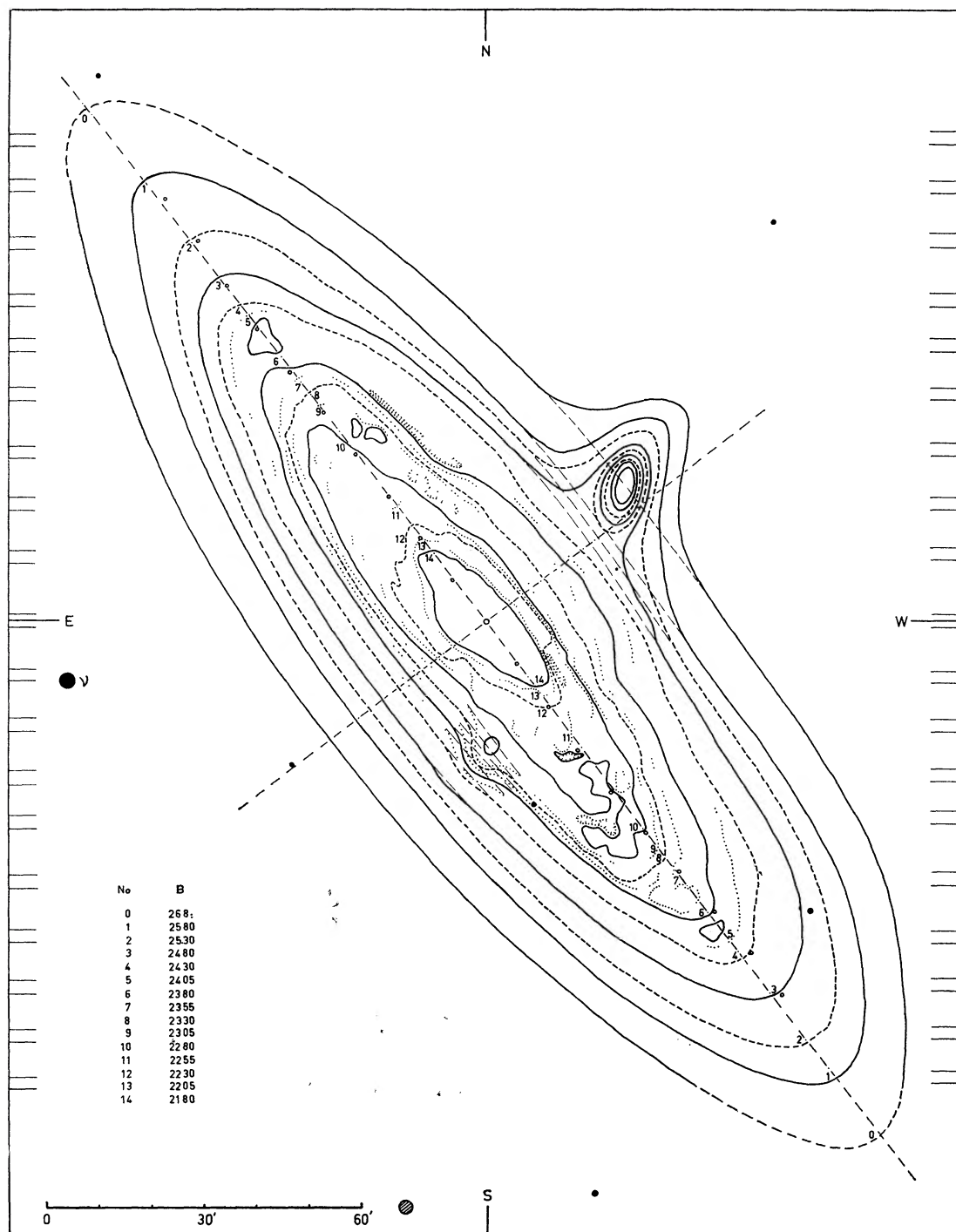


FIG. 3.—Isophotes of M31 in blue light. The small circles define the adopted major axis in p a. $37^{\circ}7'$. The declinations of the scans are marked on the margins; a few bright stars are shown. The size of the scanning hole is represented by the hatched disk. The unnumbered, closed isophotes of NGC 205 correspond to Nos. 4, 6, 8, 10, and 14. B is in units of mag/sec^2 .

In the inner region ($B < 21.80$), which was not directly observed, the profiles are based on corrected data from other sources (Sec. V). For the north-preceding half of the minor axis the values in parentheses refer to the interpolated isophotes, excluding NGC 205 (cf. Fig. 3). The mean luminosity profiles (Fig. 5) are at least approximately exponential in the outer regions; the agreement is especially close for the minor axis. This property has been observed in other spirals (Patterson 1940; de Vaucouleurs

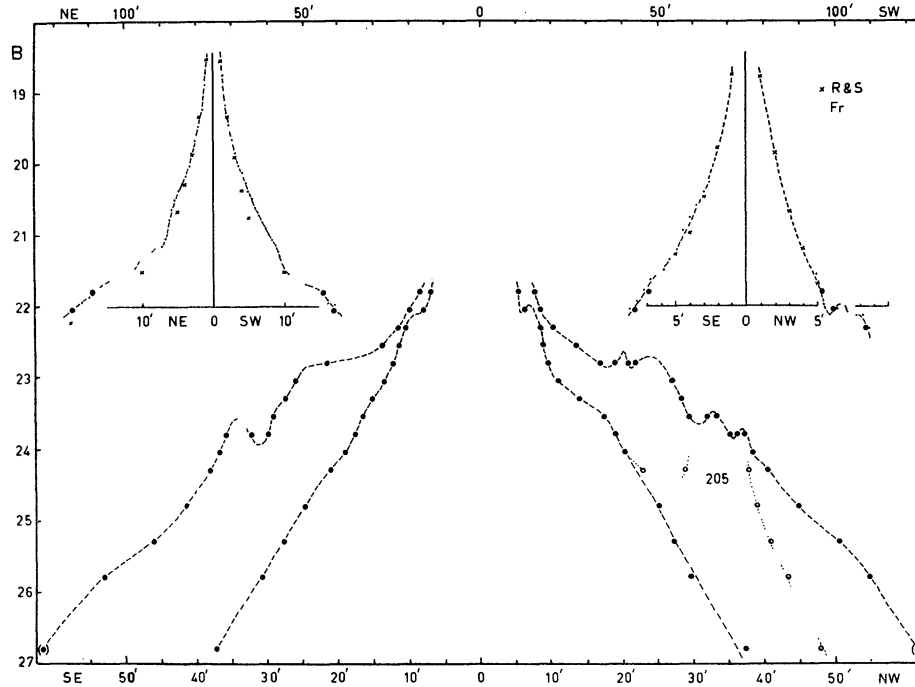


FIG. 4.—Luminosity distribution along the main axes. *Major axis*: upper curve, scale at top; *minor axis*: lower curve, scale at bottom. Surface brightness B in mag/sec². *Insets*: inner regions of major axis (*left*) and minor axis (*right*), according to the corrected data of Redman and Shirley (1937) and Fricke (1954).

TABLE 3

LUMINOSITY PROFILES OF MAJOR AND MINOR AXES

Isophote	B	$a(\text{SW})$	$a(\text{NE})$	Mean	$b(\text{SE})$	$b(\text{NW})$	Mean	$\langle b/a \rangle$
14	21.80	15'.4	17'.3	16'.35	6'.9	5'.3	6'.1	0.373
13	22.05	16'.9	20'.0	18'.45	7'.9	6'.1	7'.0	380
12	22.3	20'.5	23'.2	21'.85	10'.6	8'.4	9'.5	435
11	22.55	27'.0	27'.8	27'.4	11'.6	8'.8	10'.2	372
10	22.8	(39'.2)	43'.2	41'.2	12'.4	9'.4	10'.9	265
9	23.05	54'.0	52'.1	53'.05	13'.6	10'.9	12'.25	231
8	23.3	56'.5	55'.0	55'.75	15'.3	13'.9	14'.6	262
7	23.55	(63'.2)	58'.5	60'.85	16'.6	17'.4	17'.0	279
6	23.8	(72'.3)	(65'.8)	69'.05	17'.7	18'.9	18'.3	265
5	24.05	76'.4	73'.7	75'.05	19'.1	20'.2	19'.65	262
4	24.3	80'.8	76'.1	78'.45	21'.1	22'.8	21'.95	280
3	24.8	89'.5	82'.8	86'.15	24'.8	38'.9(25'.1)	(24'.95)	293
2	25.3	101'.0	92'.0	96'.5	27'.7	40'.8(27'.2)	(27'.45)	284
1	25.8	109'.5	106'.0	108'.25	30'.9	43'.3(29'.5)	(30'.2)	279
0	26.8	123'.:	123'.4:	123'.2:	37'.2:	47'.9(37'.4:)	(37'.3:)	0.30:

1957*a*, *b*), and it may be characteristic. The average luminosity gradients in these outer regions are $G = 2.70$ mag/deg (major axis) and $g = 9.40$ mag/deg (minor axis).

If we assume with M. Schmidt (1957*b*) a true distance modulus $m_0 - M = 24.0$, the distance of M31 is $D = 0.63$ Mpc and $l^\circ = 11$ kpc; the mean apparent luminosity gradient along the major axis is, then, $d \log I/da = -0.10/\text{kpc}$. For comparison, corresponding values in the Large Cloud (de Vaucouleurs 1957*a*) and M33 (Patterson 1940) are -0.25 kpc^{-1} and 0.24 kpc^{-1} , if the true distance moduli are 19.0 and 24.0 mag., respectively.

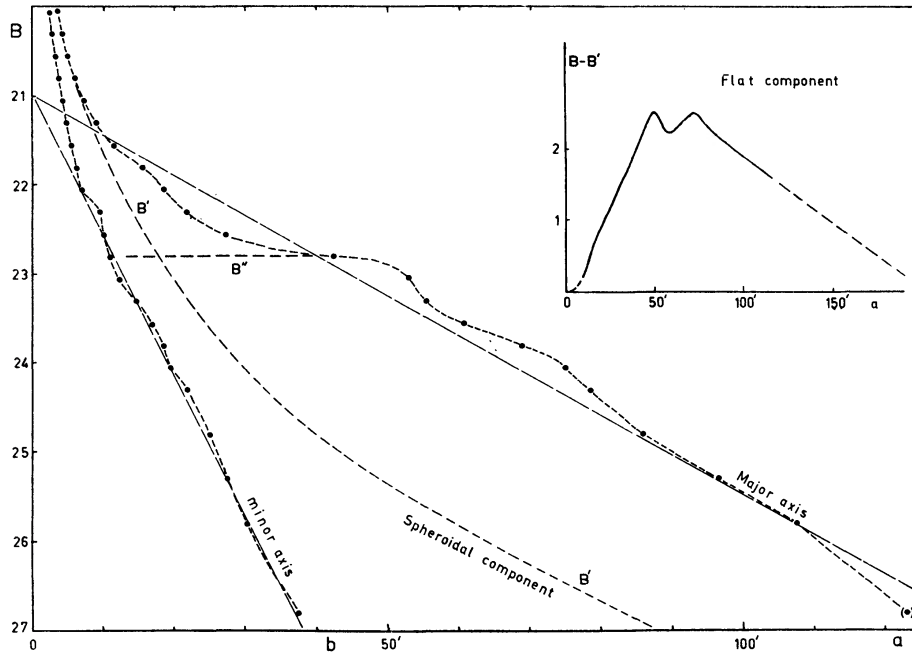


FIG 5—Mean luminosity profiles of the main axes. Decomposition of the profile of the major axis into a spheroidal component $B'B'$ and a flat component $B - B'$ (inset). The straight dashed lines correspond to 2.70 mag/deg (major axis) and 9.40 mag/deg (minor axis) (See text, Sec IV (c), and compare with Fig 10).

d) Axial Ratio

The mean axial ratios $\langle b/a \rangle$ listed in the last column of Table 3 refer to the corrected isophotes only. These ratios apply to the axes $2a$ and $2b$ defined by the intersections of the isophotes with the main axes of the nebula, not to the axes of the best-fitting ellipses. However, the distinction is significant mainly in the case of the innermost isophotes ($B < 21.8$), whose axes are in a distinctly different position angle; this phenomenon, which is connected with the incipient barred spiral structure in M31, has been discussed by Lindblad (1956).

The run of $\langle b/a \rangle$ against a is illustrated in Figure 6. The minimum axial ratio $(\langle b/a \rangle)_m \approx 0.25$ is reached near $a \approx 50'$, where $B \approx 22.5$ mag/sec²; this distance corresponds closely to the outline of the “classical” region of the nebula marked by the stronger spiral arms. This axial ratio is consistent with a tilt angle of the equatorial plane to the line of sight, $i \leq 14^\circ 5'$; if the actual tilt angle is $i = 12^\circ 3'$ (Baade, quoted by M. Schmidt 1957*b*), then the true axial ratio of the flat component of M31 is

$$q = \left[\frac{(b/a)^2 - \sin^2 i}{\cos^2 i} \right]^{1/2} = 0.042.$$

This value of q gives, for the thickness of the spiral structure, $2h = 2aq \approx 0.8$ kpc, a very plausible value if compared with the value $2h \approx 0.5$ kpc in the smaller galactic system (M. Schmidt 1957*a*).

The average value in the outer exponential regions (Fig. 5) is $\langle b/a \rangle = 0.287$, which gives $q = 0.056$ if $i = 12^\circ 3'$; this is in fair agreement with the values (0.07–0.09) quoted by Wyse and Mayall (1942) for a number of Sb spirals seen edgewise. The contradiction noted by M. Schmidt (1957*b*) between tilt angle and axial ratio of the isophotes according to the data of Redman and Shirley (1937) was obviously due to systematic errors in their photometry (Sec. V).

V. COMPARISON WITH OTHER DATA

A check on the zero point of the magnitude scale was obtained through a comparison with independent photoelectric determinations of the mean surface brightness of a number of small patches measured through a 28" diaphragm at the prime focus of the

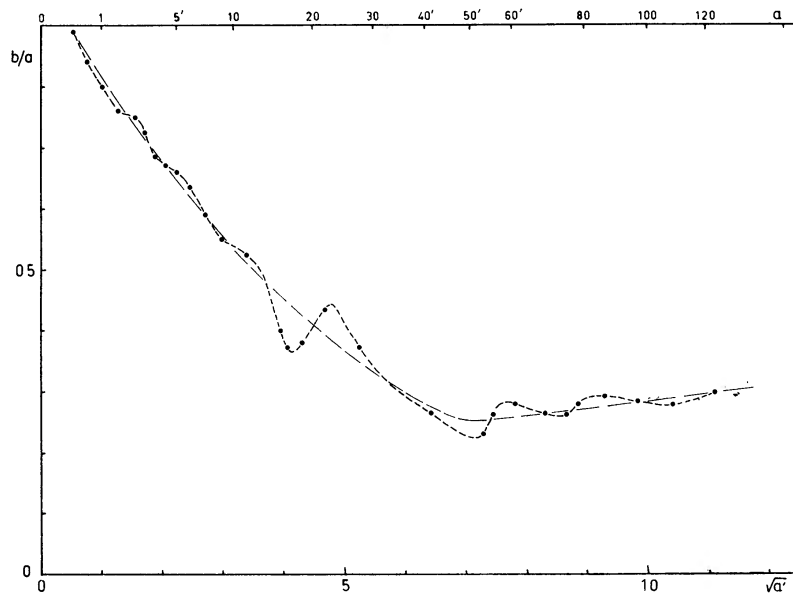


FIG. 6.—Mean axial ratio b/a of isophotes as a function of a

200-inch telescope (Baum and Schwarzschild 1955). The patches were accurately located on a Palomar 48-inch Schmidt photograph, and the corresponding magnitudes were read off by interpolation between the isophotes of Figure 3. This comparison indicates that both series of observations are closely on the same system; the straight mean of all seven fields gives $\langle B'_1 \rangle = 25.80 \pm 0.05$ (p.e.) or, rejecting fields 6 and 7, which are in a region close to NGC 205, where the luminosity gradient is very steep, $\langle B'_1 \rangle = 25.90 \pm 0.04$ (p.e.). The direct calibration (Sec. III) gave $B_1 = 25.784 \pm 0.009$ (p.e.), and the rounded-off value $B_1 = 25.80 \pm 0.01$ (p.e.) was consequently adopted for the present investigation.

The comparison with the photographic observations of Fricke (1954) is illustrated in Figure 7; the agreement is generally good, except in a few regions where the slightly different definitions of the axes and spectral ranges lead to some apparent discrepancies. Neglecting small differential color effects, the magnitudes m_{431} will be reduced to the present system of B magnitudes in the range $19.5 < m_{431} < 22.5$ through the relation

$$B = m_{431} - 0.20 . \quad (1)$$

The photographic observations of Redman and Shirley (1937) are the only ones that cover the nuclear regions with adequate resolution, but their large systematic errors must be corrected. Comparisons with the photoelectric data of Stebbins and Whitford (1934), Baum and Schwarzschild (1955), and the present observations indicate the presence of a well-defined *scale error*, which may be written

$$P - m_{pg} = +0.13 (m_{pg} - 16.2). \tag{2}$$

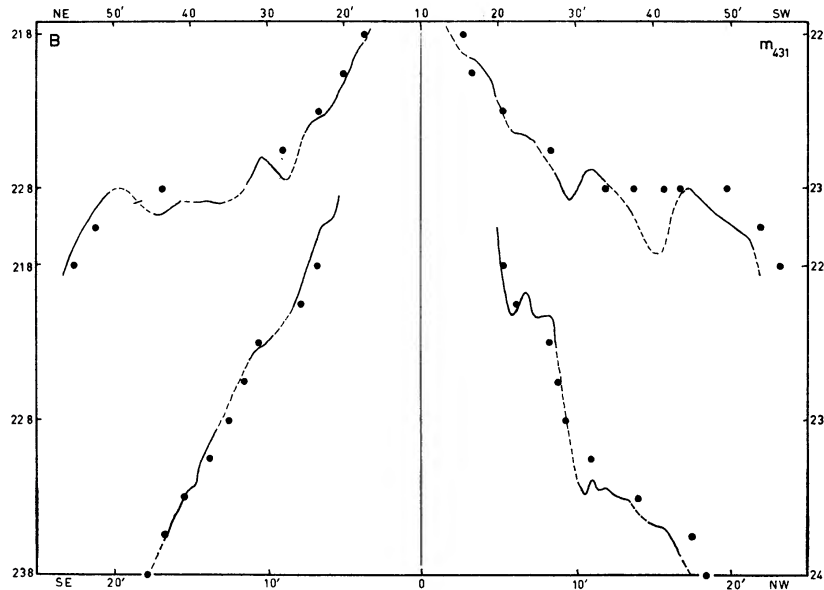


FIG. 7—Comparison with data of Fricke (1954). The luminosity profiles according to Fricke (*continuous curves*, scale at right) are compared with the photoelectric observations (*dots*, scale at left) for the major axis (*upper curve*, scale at top) and minor axis (*lower curve*, scale at bottom).

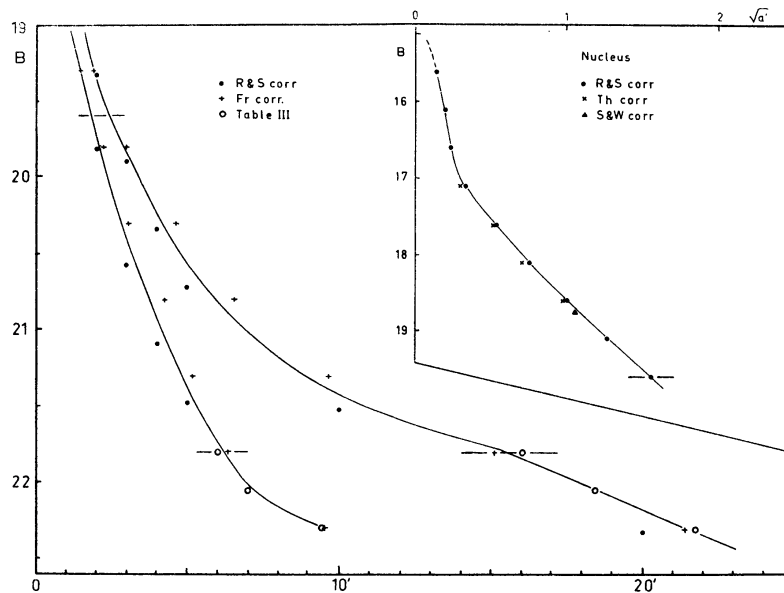


FIG. 8—Adopted luminosity profiles in inner region. *Nucleus*: major axis for $B < 19.6$ from the corrected data of Redman and Shirley; Thiessen; Stebbins and Whitford. Abscissae are \sqrt{a} with a in minutes of arc. *Inner region*: major and minor axes for $19.6 < B < 21.8$ from the corrected data of Redman and Shirley and of Fricke; for $B > 21.8$, photoelectric data from Table 3.

The adopted luminosity profiles of the nuclear regions derived from Redman and Shirley's Figure 2, including E. G. Williams' measures on Mount Wilson plates for $r < 0.1$, after correction through relation (2), are illustrated in Figure 8, together with some independent photoelectric measures by Thiessen (1956) that indicate a satisfactory agreement; a further check based on integrated magnitudes is given in Section VI. The data of Thiessen, secured by means of a 7"8 diaphragm at the photographic focus of the Hamburg 60-cm refractor, refer to distances $b < 1.0$ along the minor axis, but it is easy to compute the corresponding distances along the major axis. A value quoted by Stebbins and Whitford (1934), $P_e = 18.6$ mag/sec², equivalent to $P \approx 18.65$ (cf. Sec. VI) at 1' from the nucleus probably refers to points on the hour circle through the nucleus, the corresponding distance on the major axis, $a = 1.1$, is also plotted in Figure 8.

Finally, the data must be converted to the standard system. Johnson (1955) has listed a number of relations between various "international" P systems and the B system; fortunately, for a star having the mean color index $\langle(B - V)\rangle = +0.9$ of M31 (Sec. VIII), all relations lead to very nearly the same difference, $B - P$; in the mean,

$$\langle B - P \rangle = +0.10 \pm 0.01 \text{ (p.e.)} . \quad (3)$$

The adopted values for the luminosity profiles of the nuclear region are collected in the first 18 lines of Table 4. It is obvious that new and more accurate determinations are needed in this region, but the accuracy of the tabulated values is quite sufficient for the present purpose, as will be shown in the next section.

VI. INTEGRATED MAGNITUDES AND EFFECTIVE DIMENSIONS

a) Integrated Magnitudes

The integrated magnitudes of the nuclear region measured through small holes afford useful checks of the adopted luminosity profiles. Stebbins and Whitford (1934) quote for the integrated magnitude within $r = 1.0$ a value $P_e = 7.9$; allowance for color and zero-point corrections (de Vaucouleurs 1956*a*, 1957*b*) gives $B \approx 8.05$ ($r = 1.0$).

The integrated magnitudes and colors of the nucleus through the 5.5- and 10-mm holes were determined during the present series of observations, with results given in the accompanying table. The second value is confirmed by an unpublished measure

r	B	$B - V$	$U - B$	n
1.15	7 81	+1 02	+0 66	1
2.08	7 11	+1 02	+0 65	4

of Johnson in 1955, viz., 7.11, +1.02, and +0.62.

Integration of the adopted luminosity profiles of Table 4 leads to the computed values $m(r)$ and O - C residuals in the accompanying table. The agreement is as good as

$r = (ab)^{1/2}$	$m(r)$	O - C
1.0	8 01 ₅	+0 03 ₅
1.15	7 83 ₅	- 02 ₅
2.08	7 11	0 00

could be expected and checks the correctness of the magnitude scale adopted in Table 4, at least in the range $17.1 < B < 19.6$, which contributes nearly 99 per cent of the integrated luminosity out to $r = 2.08$.

From the last isophote $B = 19.60$, where $m(r) = 7.13$, to the inner photoelectric isophote $B = 21.80$ the integration was carried forward by means of both Redman and Shirley's and Fricke's data, corrected as explained in Section V; in this range the two sets of data differ by as much as 0.2 mag., the former being the fainter. Since there is no clear choice, a mean curve was adopted, and the area of the isophotes, assumed elliptical, was computed as shown in Table 4. The area thus computed of the last

TABLE 4*
ADOPTED LUMINOSITY PROFILES AND INTEGRATED LUMINOSITIES

B	$\log I$	\bar{I}	ΔA	A	$\bar{I} \times \Delta A$	$\Sigma I \Delta A$	$m(r)$	$k(r)$	$2a \times 2b$	b/a	a/a_e
15 1:	2 96:			0 000		0 0			0'0 0'0	(1)	(0)
15 6:	2 76	725:	0 001	0 001	0 7:	0 7:			0'04 0'04	(1)	(0)
16 1:	2 56	457	0 002	0 003	0 9:	1 6:	13 10	0 000 _s	0'07 0'07	(1)	0 001
16 6	2 36	288	0 006	0 009	1 7	3 3	12 315	000 ₇	0'11 0'10 ₅	0 95	0 001 ₅
17 1	2 16	182	0 025	0 034	4 5	7 8	11 385	001 ₅	0'22 0'20	91	0 003
17 6	1 96	115	0 185	0 219	21 3	29 1	9 95	006	0'56 0'50	89	0 008
18 1	1 76	72 5	0 613	0 832	44 5	73 6	8 945	015	1'12 0'94	84	0 016
18 6	1 56	45 7	1 68	2 51	76 8	150 4	8 185	030	2'0 1'6	80	0 028
19 1	1 36	28 8	3 64	6 15	104 8	255 2	7 59	051	3'2 2'5	76	0 045
19 6	1 16	18 2	7 45	13 5	135 5	390 7	7 13	078	4'8 3'6	75	0 068
19 8	1 08	13 2	5 7	19 2	75 3	466 0	6 94	093	5'8 4'2	72 ₅	0 082
20 05	0 98	10 7	7 2	26 4	77	543	6 775	108	7'0 4'8	68 ₅	0 099
20 3	0 88	8 5	10 5	36 9	89	632	6 61	126	8'4 5'6	67	0 118
20 55	0 78	6 75	15 0	51 9	101	733	6 45	146	10'0 6'6	66	0 141
20 8	0 68	5 37	19 8	71 7	107	840	6 305	167	12'0 7'6	635	0 169
21 05	0 58	4 26	27 0	98 7	115	955	6 16	190	14'6 8'6	59	0 206
21 3	0 48	3 39	38 3	137 0	130	1085	6 02	216	17'8 9'8	55	0.250
21 55	0 38	2 69	62	199	167	1252	5 865	250	23'0 11'0	525	0 324
21 8	0 28	2 14	101	300	216	1468	5 695	293	31': 12'4	40	0 436
22 05	0 18	1 70	85	385	144	1612	5 59	321	37' 14'	38	0 520
22 3	0 08	1 35	225	610	304	1916	5 405	382	43'5 19'	435	0 612
22 55	\bar{I} 98	1 07	410	1020	439	2355	5 18	470	54'5 20'	365	0 768
22 8	\bar{I} 88	0 85	590	1610	501	2856	4 97	569	85': 22'	26:	1 20:
23 05	\bar{I} 78	0 676	570	2180	385	3241	4 835	646	106' 24'5	23	1 49
23 3	\bar{I} 68	0 537	345	2525	185	3426	4 775	684	111' 29'5	265	1 56
23 55	\bar{I} 58	0 427	565	3090	241	3667	4 70	731	121'5 34'	28	1 71
23 8	\bar{I} 48	0 339	550	3640	186	3853	4 645	767	138' 37'	27	1 94
24 05	\bar{I} 38	0 269	995	4595	257	4110	4 575	820	150' 39'	26	2 11
24 3	\bar{I} 28	0 214	805	5400	172	4282	4 53	854	157' 43'5	275	2 21
24 8	\bar{I} 08	0 151	1500	6900	226	4508	4 48	900	172' 50'	29	2 42
25 3	$\bar{2}$ 88	0 096	1640	8540	157	4665	4 44	930	193' 55'	285	2 72
25 8	$\bar{2}$ 68	0 060	1910	10450	114	4779	4 415	954	215' 60'5	28	3 03
26 8	$\bar{2}$ 28	0 030	4150	14600	125	4904	4 385	0 978	(245') 75':	(0 305)	
∞						5020	4 36	(1)			

* An arbitrary unit of $I = 1.00$ for $B = 22.50$ is used; area A is in square minutes of arc $B < 19.6$, Redman and Shirley corrected; $19.6 < B < 21.8$, same and Fricke; $B > 21.8$, Table 3

contour, $B = 21.80$, checks satisfactorily with the direct planimetry of the first photoelectric isophote.

Two further checks by means of integrated magnitudes are possible in this section; according to Whitford (1936), the integrated magnitudes within circular diaphragms of diameters $2r = 24'$ and $30'$ are $P_e = 5.45 \pm 0.03$ and 5.35 ± 0.04 , respectively, or, after reduction to the B system as above, 5.60 and 5.50. By planimetry of the isophotes in Figure 3, the corresponding computed $m(r)$ are obtained:

r	$m(r)$	O-C
12'	5.59	+0.01
15'	5.42 ₅	+0.07 ₅

Beyond $B = 21.80$ mag/sec², planimetry of the photoelectric isophotes leads to the results listed in the third section of Table 4. The integrated magnitude within the last reliable isophote, $B_1 = 25.80$ mag/sec², is $m_1(B) = 4.41_5$; out to the last observed contour, $B_0 \approx 26.8$ mag/sec², it is $m_0(B) = 4.38_5$. This value is in good agreement with Holmberg's (1950) measured with the Mount Wilson 10-inch refractor, $m_{pg} = 4.33 \pm 0.03$ (m.e.), corresponding to $m(B) \approx 4.4$. In view of the inclusion of some ultraviolet in the photographic system used by Holmberg, a comparison with the photovisual magnitude $m_{pv} = 3.47 \pm 0.03$ (m.e.) may be more appropriate, since it is generally found that $IP_v = V$, with the adopted mean color of M31, $\langle(B - V)\rangle = +0.91$ (Sec. VIII), this m_{pv} leads to $B = 4.38$, in very good agreement with the present determination.

The probable error of the integrated magnitude depends on the p.e. of B_1 , on the p.e. of the mean reference level, and on the integration errors. With all factors taken into account, the resulting p.e. of the integrated magnitudes may be estimated at ± 0.02 mag.

Hence the integrated magnitude of M31, its companions excluded, down to the surface-brightness level, $B_0 = 26.8$ mag/sec² ($2a \times 2b = 245' : \times 75' ; A = 4.0$ sq deg) is

$$m_0(B) = 4.39 \pm 0.02 \text{ (p.e.) .}$$

Including M32 ($B = 9.15$) and NGC 205 ($B = 9.0$) merely adds 1.3 and 1.4 per cent, respectively, for a total correction of -0.03 mag. Extrapolation to infinity to include the very faint outermost extensions of surface brightness less than the threshold ($B > 26.8$ mag/sec²) adds a quantity of the same order, which is readily estimated if one assumes that the validity of the exponential luminosity law (Fig. 5) extends beyond the observed range; the total magnitude thus computed is only 0.02–0.03 brighter than m_0 . Depending on the definition adopted, a number of slightly different values ranging from 4.39 to 4.34 may therefore be given for the integrated magnitude of M31. For definiteness, the total magnitude (extrapolated, excluding companions)

$$m_T(B) = 4.36 \pm 0.02 \text{ (p.e.) ,}$$

may be adopted here.

b) Effective Dimensions

The fraction $k(r) = L_r/L_T$ of the total luminosity, L_T , emitted within each isophote is given in Table 4 and is plotted in Figure 9 as a function of both B and \sqrt{a} . An alternative representation previously used (de Vaucouleurs 1957a) is a plot of $m_r - m_T$ as a function of $A^{-1/2}$. From either graph the "effective" dimensions $2a_e$ and $2b_e$ and the surface brightness, B_e , of the isophote within which is emitted half the total luminosity (de Vaucouleurs 1948) are readily obtained, viz., $2a_e = 71'$; $b_e/a_e = 0.30$; $B_e = 22.62$

mag/sec²; and $A_e = 1170$ sq min. Assuming again a distance $D = 0.63$ Mpc, the linear effective semimajor axis is $a_e = 6.5$ kpc; the corresponding figure for the Large Magellanic Cloud, if $D = 0.063$ Mpc, is $a_e = 2.7$ kpc. The maximum measured dimensions are about $4^\circ 1' = 45$ kpc for M31 and $17^\circ = 19$ kpc for the Large Cloud; in both cases $M31/LMC = 2.4$.

VII. SPHEROIDAL COMPONENT

Isophotes and direct photographs indicate the coexistence of two main components in the light of M31: (1) the region of the nuclear bulge or spheroidal component and (2) the region of the spiral arms or flat component. A general analogy between the

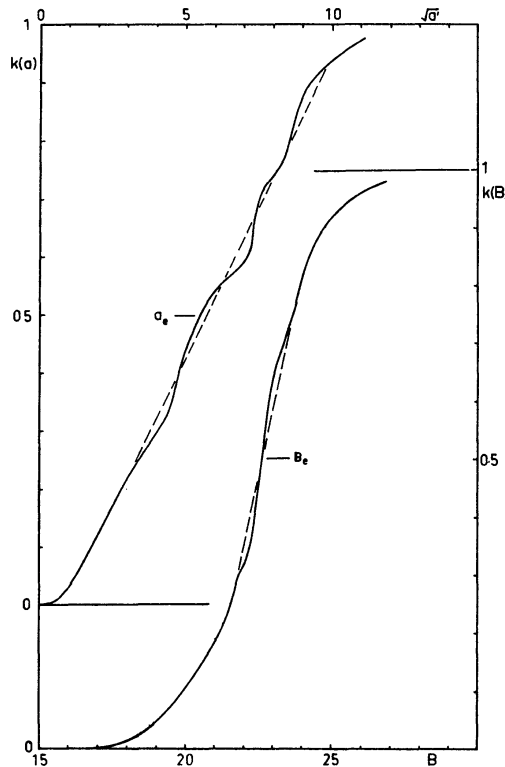


FIG. 9.—Integrated luminosity-curves. The relative integrated luminosity $k(r) = L_r/L_T$ is plotted as a function of $a^{1/2}$ (*upper curve*) and of B (*lower curve*). The effective semimajor axis $a_e = 35.5$ and effective surface brightness $B_e = 22.62$ mag/sec² are defined by $k = 0.5$.

spheroidal component and elliptical galaxies has long been assumed on the grounds of color, texture, and stellar population type. This analogy can be tested more accurately through a decomposition of the luminosity profile along the major axis into two corresponding components.

As shown by Figure 5, the region of the main spiral pattern is marked in the luminosity profile $B = f(r)$ by a plateau at $B'' = 22.8$ mag/sec², near $a \approx 35' - 45'$, so that, to a first approximation, the luminosity B' of the spheroidal component for $a < 30'$ may be taken as $B' = B - B''$. A plot of $\log B'$ against $a^{1/4}$ (Fig. 10) shows how closely the luminosity law characteristic of elliptical galaxies (de Vaucouleurs 1948, 1953) is followed by the spheroidal component of M31. This law may be written as follows:

$$\log \mathfrak{B} = -3.33 (a^{1/4} - 1) \quad (4)$$

if $\mathfrak{B} = B'/B'_e$ and $a = a'/a'_e$, where a'_e and B'_e are the effective semimajor axis and corresponding surface brightness of the spheroidal component; here $a'_e = 17'.5$, $B'_e = 22.86$ mag/sec², and $b'_e/a'_e \approx 0.6$.

The total luminosity of the spheroidal component is, by integration of equation (4),

$$L'_T = 7.215\pi B'_e a'_e b'_e \quad (5)$$

or, with the values above, $m'_T = 5.92$, and consequently $m''_T = 4.66$. It follows that the relative contributions of the spheroidal and flat components to the total luminosity of M31 in blue light are

$$L'_T = 0.24L_T, \quad L''_T = 0.76L_T.$$

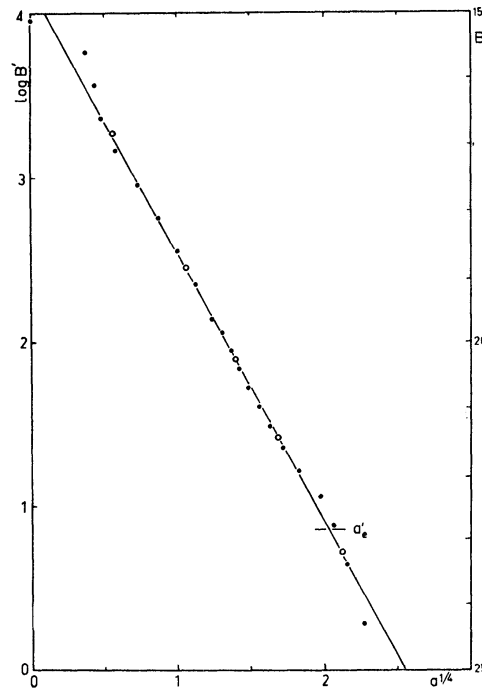


FIG. 10—Spheroidal component The surface brightness $B' = B - B''$ of the spheroidal component (cf. Fig. 5) is plotted (in arbitrary units in a log scale at left and in magnitudes, scale at right) against the fourth root of the radius (in minutes of arc). *Dots*: observed luminosity profile along major axis; *circles*: mean points The straight line expresses the ellipsoidal luminosity law; the effective semimajor axis of the spheroidal component is marked at $a'_e = 17'.5$

Because of the redder color of the nuclear region, the ratio L'/L will be slightly greater in yellow light, about 30 per cent.

If we assume that the spheroidal component pervades the whole system and follows throughout the same luminosity law (4), its contribution to the observed surface brightness may be computed; it is rather small beyond $a \approx 30'$ and up to the limit of the measurements at $a \approx 2^\circ$; as shown by Figure 5, it is everywhere from 1.5 to 2.5 mag. below the observed luminosity-curve, i.e., it contributes only from 25 to 10 per cent to the measured surface brightness in blue light. Again its contribution may be somewhat greater at longer wave lengths, and it seems possible that it is the stellar population of this component that is detected on photographs in red light (Baade 1951), showing a smooth distribution of faint stars in the outer regions. If such a large extrapolation were per-

missible, one might expect that the spheroidal component would contribute most of the light in the outermost regions beyond $a \approx 3^\circ$ or 3.5° , where the predicted surface brightness is $B \approx 29$ mag/sec² or fainter.

VIII. COLOR DISTRIBUTION

The color distribution was not determined in detail for the whole nebula, but only for a number of cross-sections.

a) *The East-West Diameter*

The east-west cross-section at the declination of the nucleus was the best observed, the B , V , U data being based on 8, 2, and 2 scans, respectively.

Comparison of the color and luminosity distributions (Fig. 11) clearly indicates that the preceding side of the nebula is both obscured and reddened; the relation may be illustrated by means of the color-luminosity asymmetry diagram (Lindblad 1941, 1942) in which the abscissae are the magnitude differences,

$$A_2 = B(-x) - B(+x),$$

and the ordinates are the color differences,

$$A_2 - A_1 = (B - V)_{-x} - (B - V)_{+x},$$

for points at equal distances ($-x$, $+x$) from the nucleus on the obscured and unobscured sides (Fig. 12, *a*). The accuracy is low in the outer parts, but in the range $9' < |x| < 22'$ ($21.8 < B < 23.8$), corresponding approximately to $7' < |b| < 17'$ on the minor axis, the asymmetry-curve is similar to those of NGC 4216 and 7331 (Lindblad 1941, 1942; Elvius 1956) and therefore of Lindblad's class II; this result could be expected in view of the close similarity of type and tilt of the three spirals. It follows that the obscured and reddened side of M31 is also the near side, as is unquestionably the case for NGC 7331 (de Vaucouleurs 1958*a*) and the arms are trailing in the rotation.

b) *The Minor Axis*

The color distribution along the minor axis was not observed directly, but several published data are collected in the upper part of Figure 13, as follows:

$$\text{Stebbins (1950): } B - V \approx +1.00 + \left(\frac{\Delta C_5}{2.13} \right), \quad \text{where } C_5 = m_{425} - m_{750};$$

$$\text{Fricke (1954): } B - V \approx +0.10 + \frac{C_r}{1.5}, \quad \text{where } C_r = m_{431} - m_{624};$$

$$\text{Thiessen (1956): } B - V \approx +0.10 + (P - V).$$

For comparison, the values of $B - V$ measured along the east-west diameter are added, with distances approximately reduced to the minor axis following the isophotes. The various data are in general agreement except in the nucleus ($b < 1.0'$), where new observations are needed.

There is a conspicuous reddening in the main dark lane about $5'-6'$ northwest of the nucleus ($B - V \approx +1.15$); the next spiral arm about $7'-8'$ northwest is also strongly reddened on its inner edge ($B - V \approx +1.05$) but appears bluer on its outer edge ($B - V \approx +0.95$). By contrast, the spiral arm about $10'-11'$ southeast of the nucleus

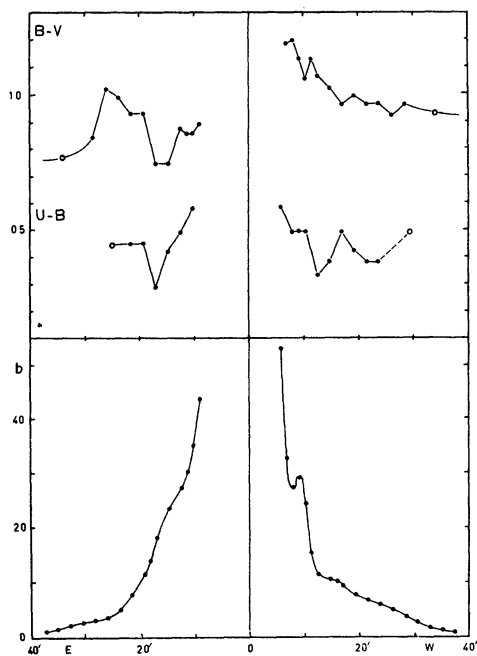


FIG 11.—Color and luminosity profiles of the east-west central section. The luminosity profile in blue light (*lower curve, in b units*) is compared with the color profiles $B - V$, $U - B$ (*upper curves*)

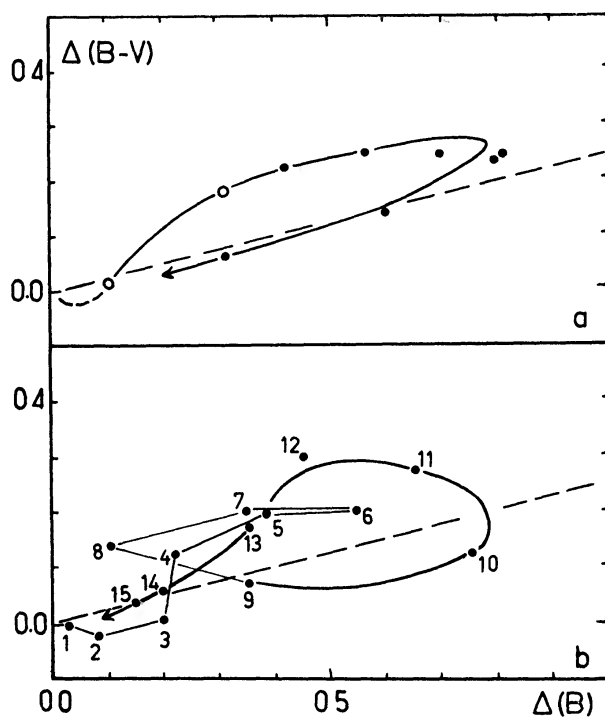


FIG. 12 —Color-luminosity asymmetry-curves *a*, East-west central section from Fig 11; open circles represent data by Hoag *b*, Minor axis from Fig 13. The numbers denote distances to the nucleus in minutes of arc. The interrupted lines correspond to the relation $\Delta(B - V) = \Delta(B)/4$

is only slightly reddened on its inner edge ($B - V \approx +0.85$), and its outer edge is much bluer ($B - V \approx +0.75$).

Combination of the color-curve with the luminosity-curve of the minor axis leads to the asymmetry-curve shown in Figure 12, *b*; while the curve is still generally of class II (or perhaps III), it is obvious that a great deal of fine structure is present and that, in general, the interpretation of such curves is not simple.

c) The Major Axis

The color distribution along the major axis was not observed directly, except at $\delta_N \pm 30'$ and $\delta_N \pm 60'$; the published data are also collected in the lower part of Figure 13. There is a notable discrepancy of about 0.1 mag. between the reduced colors of Fricke and the photoelectric values, although the same reduction formula was used that leads to good agreement for the minor axis. Also the variation of about 0.1 mag. in the mean color between the two halves of the major axis suggested by the photographic and photoelectric data will require verification.

d) Sections at $\delta_N \pm 30'$ and $\delta_N \pm 60'$

In Figure 14 are shown the variations of $\langle \bar{B} \rangle$ and $\langle (B - V) \rangle$ for the two east-west sections $30'$ north and south of the nucleus; the abscissae in each case are measured from the intersection of the major axis with the scans. It appears that, within the region occupied by the spiral structure, $\langle (B - V) \rangle \approx +0.85$, with minima around $+0.8$ in the arms, while in the faint outer regions $\langle (B - V) \rangle \approx +1.0$, which is in sufficient agreement with the value determined for the central scan. However, the accurate spot measurements of Baum and Schwarzschild (1955) along the minor axis give $\langle (B - V) \rangle = +0.87$ in the outer parts (Sec. V).

Excluding the outer regions, where the y and u deflections are less than 2 units, the straight means of $B - V$ and $U - B$ are given in the accompanying table.

$\delta - \delta_N$	Range (R A)	$\langle B - V \rangle$	$\langle U - B \rangle$
+60' . .	30'	+0 60: (13)	
+30' ..	63'	+ .87 (28)	Rej.
0 . . .	70'	+ 90 (19)*	+0 44 (12)*
-30' . .	68'	+ 94 (31)	+0 49 (19)
-60' . .	32'	+0 81: (14)	

* Excluding the central section within $\pm 13'$ from the nucleus; in this section $\langle (B - V) \rangle \approx +1.00$ and $\langle (U - B) \rangle \approx +0.55$ (cf Fig 11)

e) Mean Colors

An exact computation of the over-all average color is not possible with the data at hand; however, a rough division of the nebula into three regions, each contributing about one-third of the integrated blue luminosity (Table 4) is given in the accompanying table.

Region	Range	$\langle B - V \rangle$	$\langle U - B \rangle$
Core (spherical component)	$B < 22$ mag/sec ²	+1 0	+0 6
Lens (flat component)	22-23	+0 85	+ 4
Envelope (exponential tail)	$B > 23$	+0 9	+ 5
Mean		+0 91	+ 50
p e		$\pm 0 02$	$\pm 0 02$

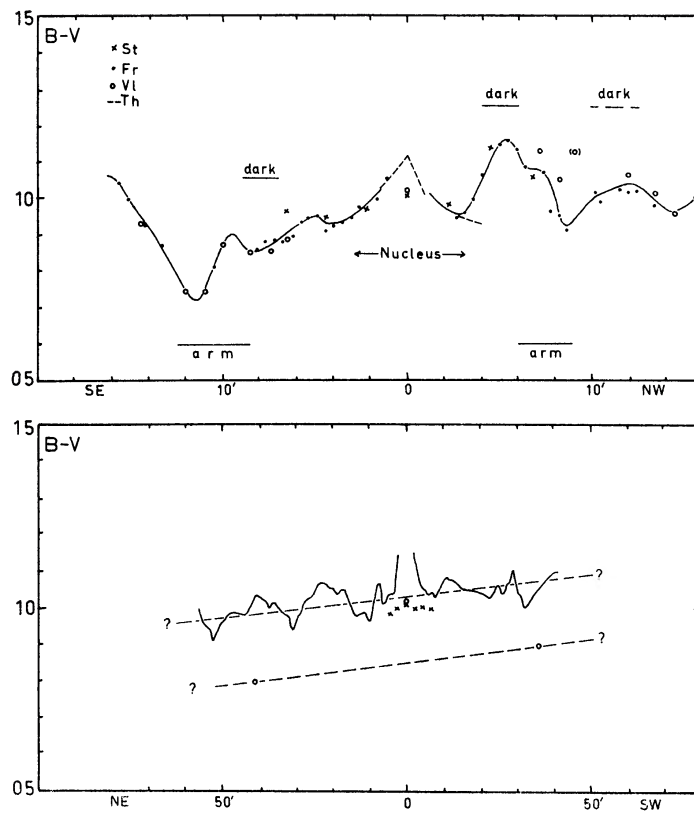


FIG 13—Color distributions along the main axes *Above*: minor axis from data by Stebbins, Fricke, and Thiessen, and from Fig 11 *Below*: major axis from data by Fricke (*continuous curve*), Stebbins (*crosses*), and the present observations (*circles*)

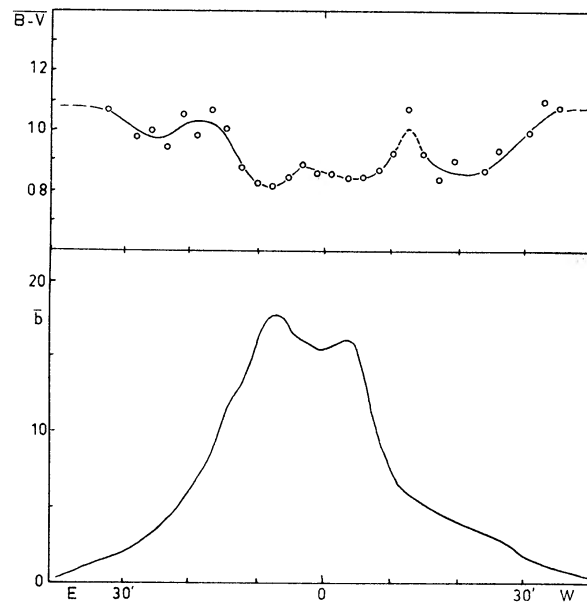


FIG 14.—Mean color and luminosity profiles of the east-west sections 30' north and south of the nucleus *Above*: color-curve (mean points only); *below*: luminosity-curve in b units The origin of abscissae is the major axis

IX. MASS/LUMINOSITY RATIOS

Table 5, adapted from M. Schmidt's paper (1957*b*), gives in columns 1 and 2 the distance a from the center in degrees and kpc; in column 3 the mass surface density $\sigma'_{\mathfrak{M}}$ projected on the equatorial plane in solar masses per square parsec; in column 4 the observed B surface brightness $\sigma_{\mathfrak{L}}$ expressed in solar units per square second, assuming, as before, $m - M = 24.25$, $m - m_0 = 0.25$, and $M(\text{sun}) = +5.47 (B)$ (Stebbins and Kron 1957); in column 5 the observed axial ratio b/a of the isophotes; in column 6 the mass surface density projected on the sky $\sigma_{\mathfrak{M}} = \sigma'_{\mathfrak{M}}(b/a)$ expressed in solar masses per square second of arc; in column 7 the apparent mass/luminosity ratio $f = \sigma_{\mathfrak{M}}/\sigma_{\mathfrak{L}}$ at $r = a$; in column 8 the fraction $k(\mathfrak{M})$ of the total mass within $r = a$; in column 9 the fraction $k(\mathfrak{L})$ of the total luminosity within $r = a$; and in column 10 the mean apparent mass/luminosity ratio $\langle f \rangle = \langle \mathfrak{M}/\mathfrak{L} \rangle$ within $r = a$.

TABLE 5
MASS/LUMINOSITY RATIOS*

a		$\sigma'_{\mathfrak{M}}$ (\odot/pc^2)	$\sigma_{\mathfrak{L}}$ (\odot/\square'')	b/a	$\sigma_{\mathfrak{M}}$ (\odot/\square'')	$\mathfrak{M}/\mathfrak{L}$ ($r=a$)	$k(\mathfrak{M})$ (Per Cent)	$k(\mathfrak{L})$ (Per Cent)	$\langle \mathfrak{M}/\mathfrak{L} \rangle$ ($r \leq a$)
1° (1)	kpc (2)								
0 25	2 75	982	1360	0 46:	19800	14 5	10	30	8 0
0 50	5 50	492	615	335	13700	22 3	24	46	12 5
0 75	8 25	248	530	255	9750	18 4	36	59	14 5
1 00	11 0	130	270	26	4650	17 2	45	71	15
1 50	16 5	771	70	285	2320	33	59	93	15 5
2 00	22 0	44	20	295	1390:	70:	69	98:	17
2 50	27 5	29	5 5:	0 30:	(700)	(130:)	78	99:	19:

* Mass $\mathfrak{M} = 3.4 \times 10^{11}$ suns; luminosity $\mathfrak{L}_B = 1.4 \times 10^{10}$ suns; $r_e(\text{mass}) \approx 1:15 = 12.7$ kpc; $r_e(\text{light}) \approx 0:6 = 6.5$ kpc

a) Mean Mass/Luminosity Ratio

The mass/luminosity ratio is roughly constant only in the range $0:25 = 0.3$ kpc $< r < 1:25 = 14$ kpc (Fig. 15); it increases rapidly for $r > 1:25$ and drops sharply for $r < 0:25$, reaching probably a very small value in the nucleus (Wyse and Mayall 1941); whether this is real or due to some basic weakness in the assumed dynamical model is not clear. Because the range where $f \approx \text{Const.}$ coincides with the region where the flat component dominates the light-distribution (Fig. 5), it seems plausible that, perhaps because of the neglect of the random motions, Schmidt's model does not apply to the spheroidal component (see below).

The total mass in Schmidt's model is $\mathfrak{M} = 3.38 \times 10^{11}$ suns, the total luminosity is $\mathfrak{L}_B = 1.40 \times 10^{10}$ suns if $m_T(B) = 4.36$ (Sec. VI); the mean apparent mass/luminosity ratio is, then, $\bar{f}(B) = \langle \mathfrak{M}/\mathfrak{L}_B \rangle = 24$. The effect of internal absorption is difficult to estimate; according to Holmberg (1957), a total absorption of about 1.7 mag. (P)—equivalent to 1.6 (B)—is indicated by the mean apparent surface brightness, $m + 5 \log a$ of Sb spirals when $b/a \approx 0.3$; however, his estimate does not allow for the apparent variation in the semimajor axis a with tilt angle which amounts to +60 per cent when $b/a \approx 0.3$ (de Vaucouleurs 1956*b*); this effect causes a spurious reduction of the apparent surface brightness by about 1.0 mag., so that the true absorption is only $1.6 - 1.0 = 0.6$ (B) mag. Application of this tentative correction to the apparent magnitude of M31 gives a true or absorption-free mass/luminosity ratio $\langle f_0 \rangle(B) = 13.5$. In terms of visual light, since $B - V = +0.63$ for the sun and $B - V = +0.91$ for M31 (reduced to

about +0.85 after allowing for differential absorption in the Galaxy), the apparent mean luminosity ratio is $\langle f \rangle (V) = \langle \mathfrak{M} / \mathfrak{L}_V \rangle = 19.5$. According to Holmberg (1957), the total color excess is about 0.2 mag. for $b/a \approx 0.3$, the true visual absorption is then $1.6 - 0.2 - 1.0 = 0.4$ mag., and the absorption-free mass/luminosity ratio is $\langle f_0 \rangle (V)_0 = 13.5$. The fact that $\langle f_0 \rangle (B) = \langle f_0 \rangle (V)$ results merely from the near-equality of the corrected color of M31 and of the sun.¹

b) *Masses and Mass/Luminosity Ratios of Spheroidal and Flat Components*

An independent estimate of the mass \mathfrak{M}' of the spheroidal component of M31, which presumably comprises the larger fraction of the total mass, may be derived through the virial theorem $\mathfrak{M}' = 2 \langle V^2 \rangle R/G$, where $\langle V^2 \rangle = \langle u^2 \rangle + \langle v^2 \rangle + \langle w^2 \rangle = 3 \langle w^2 \rangle$, from a value of the line-of-sight velocity dispersion (Minkowski 1954), $\langle (w^2) \rangle^{1/2} = 225$ km/sec, and the value $R = r'_e = 0.3 = 3.3$ kpc (Sec. VII). This gives $\mathfrak{M}' = 2.4 \times 10^{11}$ suns, a reasonable value.

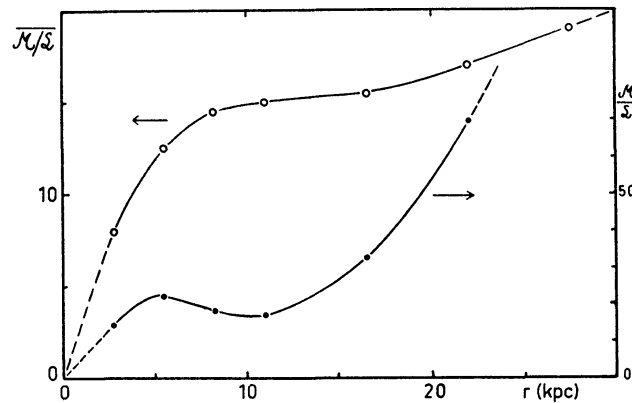


FIG 15—Apparent mass/luminosity ratio *Lower curve* (scale at right): local value at $r = a$; *upper curve* (scale at left): integrated or mean value within $r = a$. The luminosity refers to blue light and is not corrected for internal absorption effects

Since the total luminosity of the spheroidal component is $L' = 0.24 L_T$ (Sec. VII), the apparent mass/luminosity ratio is $\langle f' \rangle (B) = 70$. Because most of the light is emitted in the nuclear regions that are less obscured than the bulk of the spiral, the absorption-free ratio will be only slightly lower, perhaps $\langle f' \rangle (B) \approx 60$.

If this simplified analysis is valid, the mass of the flat component may be $\mathfrak{M}'' = \mathfrak{M} - \mathfrak{M}' = 1.0 \times 10^{11}$ suns, and since $L'' = 0.76 L_T$, $\langle f'' \rangle (B) = 9$ or, correcting again for internal absorption, $\langle f_0'' \rangle (B) \approx 5$. This is a plausible value; in the case of M33, where the flat component is probably dominant, corresponding values are $\mathfrak{M} \approx 10^{10}$ suns (Dieter 1957), $L_T(B) \approx 1.6 \times 10^9$ suns, and $\langle f'' \rangle (B) = \mathfrak{M} / \mathfrak{L}_B \approx 6$; internal absorption corrections may reduce this value to $\langle f_0 \rangle \approx 4$ or 5.

A comparison between H I intensities as measured by the integrals of line profiles (Figs. 8 and 9 in van de Hulst *et al.* 1957) and the luminosity profiles (Figs. 4 and 5) indicates a general similarity with the *relative* intensity distribution of the flat component; in particular, the main H I maxima near $r \approx 50'$ correspond closely with the main spiral arms. A similar correlation with the distribution of supergiant stars has been pointed out by van den Bergh (1958). The *absolute* radial decrease of the luminosity,

¹ If the apparent distance modulus of M31 is increased by +0.35 mag to 24.6 (Th Schmidt 1957), without changing the absorption, \mathfrak{M} will be multiplied by 1.38, \mathfrak{L} by $(1.38)^2$, and $\mathfrak{M}/\mathfrak{L}$ divided by 1.38, so that, on present evidence, the most probable value of the mean absorption-free mass/luminosity ratio of M31 may be about 10.

however, is much steeper than that of hydrogen, as was also observed in the Magellanic Clouds (Kerr and de Vaucouleurs 1956).

I am indebted to Dr. H. L. Johnson for much useful discussion of photometric problems, to Dr. A. A. Hoag for the loan of his unpublished Harvard thesis, and to Mrs. A. de Vaucouleurs for her efficient assistance in the reduction of the data.

APPENDIX I

BRIGHTNESS OF THE NIGHT SKY

The measured surface brightness of the night sky is of some interest; the mean value observed at sec $z = 1.000$ is

$$B = 22.20 \pm 0.03 \text{ mag/sec}^2 .$$

This value is about the same as was measured in 1953–1954 at Mount Stromlo (de Vaucouleurs 1957*a*) near the Small Cloud. However, according to H. L. Johnson, the scattered illumination from the nearby city lights of Flagstaff increases the surface brightness of the sky above Mars Hill (1–2 miles west) by 0.35 mag., compared with the U.S. Naval Observatory Station (5 miles southwest). The sky brightness corrected for artificial illumination, then, is $B \approx 22.5$ mag/sec², equivalent to about 145 stars of IP_0 mag. 10.0 per square degree. This figure refers to galactic co-ordinates $l = 89^\circ$, $b = -21^\circ$ and ecliptic co-ordinates $\lambda \approx 25^\circ$, $\beta \approx +35^\circ$; at the time of the observations the longitude of the sun was $\lambda_\odot \approx 240^\circ$. According to Elvey and Roach (1937), the mean galactic light at $b \approx 21^\circ$ is equivalent to 20 stars of IP_0 mag. 10 per square degree, and the mean zodiacal light at $\lambda - \lambda_\odot = 150^\circ$ and $\beta = \pm 35^\circ$ in November–December is equivalent to 90 of the same units. The combined contribution of airglow and atmospheric scattering, therefore, was

$$P_0 = 145 - 20 - 90 = 35 \text{ units} = 23.9 \text{ mag/sec}^2 (B_0 = 24.0) .$$

The darkest region of the sky should be the area around $\alpha = 14 h$, $\delta = +50^\circ$ halfway between the north galactic pole and the pole of the ecliptic, which transits slightly north of the zenith at Flagstaff; the expected brightness is

$$35 + 0 \text{ (G.L.)} + 55 \text{ (Z.L.)} = 90 \text{ units} = 22.9 \text{ (} P \text{)} \text{ or } 23.0 \text{ (} B \text{)} .$$

The corresponding minimum figure for the region of the pole of the ecliptic outside the atmosphere is 50 units = 23.5 (P) or 23.6 (B).

From these figures, the zodiacal light appears to be the main obstacle to accurate photometry of faint extended surfaces, and observing from above the atmosphere would improve the situation by only 1.0 mag. at the most. However, the main practical obstacle lies in the *fluctuations* of the airglow, which, over a period of 30–60 minutes and after correction for any linear trend, amount to something like ± 1 per cent (r.m.s.) of the total light, with pseudo-periods of the order of 1–3 minutes. Observing above the atmosphere or simultaneous sky monitoring would remove this cause of uncertainty and increase the accuracy several fold; the measurement of a surface brightness of the order of $B \approx 29$ mag/sec² and the detection of $B \approx 30$ mag/sec² would then appear possible.

APPENDIX II

INSTRUMENTAL AND ATMOSPHERIC SCATTERING

An important cause of possible systematic error in the photometry of faint extended objects is the light scattered at great distances by both the telescope and the atmosphere. Few reliable measurements have been published on this effect, despite its obvious theoretical and practical importance; available data from various sources have been collected and discussed by van de Hulst (1952).

Systematic observations of scattered light were obtained with the 20-inch reflector in connection with the present study of M31; the aluminum coat of the mirror was $4\frac{1}{2}$ years old and rather dirty and dusty by laboratory standards, but not unusually so compared with the ordinary

condition of many telescopes. The 5.5-mm hole = $2'3$ was used to scan in R.A. the scattered light of α Ari in the range $3' < \theta < 30'$; the curve was extended by taking spot readings with the same hole at $30'$ intervals in declination north and south of Jupiter near transit in the range $20' < \theta < 6^\circ = 360'$, the "zero" sky reading being taken at $\theta = \pm 10^\circ$ from the source. The supports of the small mirror are oriented in position angles 45° – 225° and 135° – 315° , i.e., at 45° from the scan directions. The composite scattering diagram, $\log I = f(\log \theta)$, is shown in Figure 16; the relation is a straight line of slope $d \log I / d \log \theta = -2.00$ over the whole range $3' < \theta < 360'$. In order to extend the range still further, the data of Redman and Shirley (1938) for the 36-inch Cambridge reflector, corrected for the magnitude scale error (Sec. V), are also included in Figure 16; the linear relationship is seen to extend with the same slope up to $\theta \approx 0'3$; in-

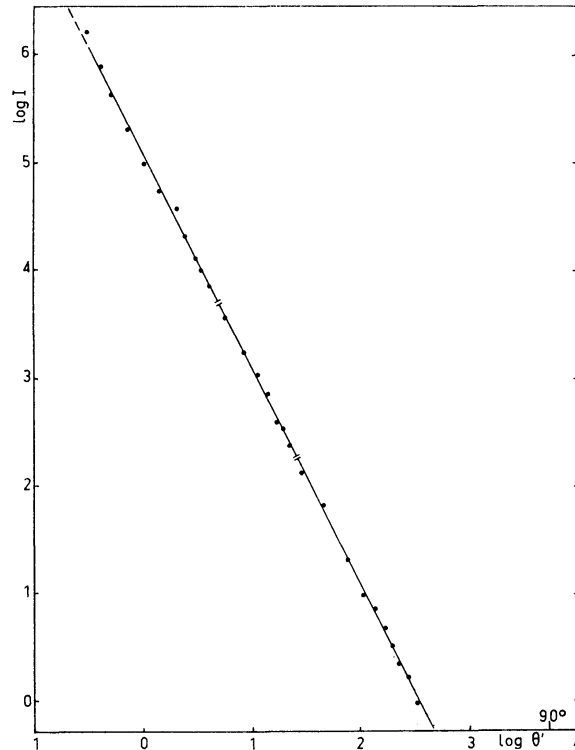


FIG. 16—Instrumental scattered light. The log surface brightness of scattered blue light is plotted against the log angular distance to the source (in minutes of arc). The relation is indistinguishable from an inverse square law in the range $0'3 < \theta < 6^\circ$, where instrumental scattering is dominant. *Upper section:* from corrected data of Redman and Shirley; *middle section:* from scans of α Ari; *lower section:* from spot readings near Jupiter.

cidentally, this result supports the applicability of correction formula (2) to all the Cambridge photometry of 1936–1938. At distances $\theta < 0'3$, diffraction in the telescope and seeing effects become increasingly important; it has been shown previously (de Vaucouleurs 1948) that in this region the luminosity distribution is well approximated by a normal error-curve.

A rough but sufficient estimate of the effect on the luminosity profiles of M31 of the light scattered from its bright nuclear regions can be obtained by assuming that it is equivalent to a central point source of magnitude $B = 5.0$; the mean observed surface brightness, B_m , along the minor axis of M31, where the effect is a maximum, is given for comparison in the table on page 488. Throughout the observed range ($r < 40'$), scattered light is from 2 to 4 mag., or six to forty times fainter than the measured brightness; actually, the effect is still smaller because the interpolated reference level allows for light scattered at $r > 50'$. This remark applies even more strongly to non-central scans for which the range of distances to the nucleus is smaller. It is concluded that, except perhaps for the outermost isophote ($B \approx 26.8$ mag/sec²),

in regions close to the minor axis the effect of scattered light on the measured surface brightness is of the order of 0.01–0.05 mag at the most, which is too small to alter the axial ratio significantly.

	<i>r</i>						
	5'	10'	15'	20'	30'	40'	60'
B_s	24.9	26.4	27.3	27.9	28.8	29.4	30.3
B_m	21.4	22.5	23.3	24.1	25.7	27.2	(30.3)*
$B_m - B_s$	-3.5	-3.9	-4.0	-3.8	-3.1	-2.2	(0.0)*

* Extrapolated

REFERENCES

- Baade, W 1951, *Pub Obs U. Michigan*, **10**, 14
 Baum, W, and Schwarzschild, M 1955, *A J*, **60**, 247
 Dieter, N. H. 1957, *Pub A.S.P.*, **69**, 356.
 Elvey, C. T, and Roach, F. E. 1937, *Ap J*, **85**, 213
 Elvius, A. 1956, *Stockholms Obs Ann*, Vol. **18**, No. 9.
 Fricke, W 1954, *Zs. f. Ap.*, **34**, 137
 Hoag, A. A. 1952, Harvard thesis (unpublished)
 Holmberg, E 1950, *Medd Lunds Obs*, Ser II, No 128
 ——— 1957, *ibid.*, (II), No 136
 Hubble, E. 1929, *Ap J*, **69**, 138
 Johnson, H. L. 1955, *Ann d'ap*, **18**, 292
 Johnson, H. L., and Morgan, W. W 1953, *Ap J*, **117**, 313
 Lindblad, B. 1941, *Stockholms Obs Ann*, Vol **13**, No 8
 ——— 1942, *ibid.*, Vol **14**, No 3
 ——— 1956, *ibid.*, Vol **19**, No 2
 Minkowski, R. 1954, in *Ann Rept. Mt Wilson-Palomar Obs 1953-54*, p 26
 Patterson, F. S 1940, *Harvard Obs Bull*, **914**, 9
 Redman, R. O., and Shirley, E. G 1937, *M N*, **97**, 416.
 ——— 1938, *ibid.*, **98**, 613
 Schmidt, M. 1957a, *B.A.N.*, **13**, No 475, 247
 ——— 1957b, *ibid.*, **14**, No 480, 17.
 Schmidt, Th. 1957, *Zs. f. Ap*, **41**, 197.
 Schwarzschild, M 1954, *A.J.*, **59**, 273
 Stebbins, J 1950, *M N*, **110**, 422
 Stebbins, J, and Whitford, A. E 1934, *Proc. Nat Acad Sci*, **20**, 93
 Thiessen, G. 1955, *Mem Soc R Sci Liège*, Ser IV, **15**, 411.
 van de Hulst, H. C 1952, in *The Atmospheres of the Earth and Planets*, ed G. P. Kuiper (Chicago: University of Chicago Press), p 69
 van de Hulst, H. C., Raimond, E., and van Woerden, H. 1957, *B.A.N*, **14**, No. 480, 1.
 Vaucouleurs, G de 1948, *Ann. d'ap*, **11**, 247
 ——— 1953, *M N*, **113**, 134
 ——— 1956a, *A J*, **61**, 430
 ——— 1956b, *Mem Commonwealth Obs.*, **3**, No 13, 16.
 ——— 1957a, *A J.*, **62**, 69
 ——— 1957, *Ann. Obs. Houga*, **2**, No. 1, 16
 ——— 1958a, *Ap J*, **127**, 487
 ——— 1958b, in *Handbuch der Physik*, Vol **53** (Berlin: Springer Verlag).
 Whitford, A. E 1936, *Ap J*, **83**, 424.
 Wyse, A. B., and Mayall, N. U. 1942 *Ap. J*, **95**, 24.